Fluorescence-Based Fouling Prediction and Optimization of a Membrane Filtration Process for Drinking Water Treatment

Ramila H. Peiris, Hector Budman, Christine Moresoli, and Raymond L. Legge
Dept. of Chemical Engineering, University of Waterloo, Waterloo, ON, Canada N2L 3G1

DOI 10.1002/aic.12684
Published online June 15, 2011 in Wiley Online Library (wileyonlinelibrary.com).

A novel fluorescence-based approach is proposed for modeling, predicting, and optimizing different fouling dynamics in an ultrafiltration (UF) process for drinking water treatment. Principal component analysis (PCA) was used to extract information in terms of principal components (PCs), related to major membrane foulant groups, from fluorescence excitation–emission matrix measurements captured during UF of natural river water. The evolution of PC scores during the filtration process was then related to membrane fouling using dynamic balances of latent variable values (PC scores). This approach was found suitable for forecasting fouling behaviors with good accuracy based solely on fluorescence data collected 15 min from the start of the filtration. The proposed approach was tested experimentally through model-based optimization of backwashing times with the objective of minimizing the energy consumption per unit amount of water produced during the filtration process. This approach was also useful for identifying fouling groups contributing to reversible and irreversible fouling. © 2011 American Institute of Chemical Engineers *AIChE J,* 58: 1475–1486, 2012
Keywords: drinking water treatment, fluorescence spectroscopy, modeling membrane fouling, principal component analysis, real-time optimization

Introduction

Membranes are widely used in drinking water applications to achieve improved removal of colloidal/particulate matter, pathogenic organisms, natural organic matter (NOM), and salinity in water. Different types of membrane systems such as microfiltration, ultrafiltration (UF), nanofiltration, and reverse osmosis are being increasingly used individually or in combination (hybrid mode) to accomplish these treatment objectives and to produce drinking water with consistent quality.[1,2] Membrane-based technology also allows a smaller footprint for the treatment facilities compared to conventional treatment processes.[3] However, membrane fouling, which is the result of the accumulation of materials (foulants) on the surface and/or in the pores of the membranes, is a major constraint when considering both the adoption and performance consistency of membrane-based treatment operations. NOM fractions, such as humic substances (HS), protein- and polysaccharide-like substances as well as colloidal/particulate matter present in water, are mainly responsible for membrane fouling in drinking water applications.[4,5] In practice, membrane fouling is controlled by implementing cleaning operation schemes that include membrane backwashing (also known as back-flushing)[6] and chemical cleaning of fouled membranes.[7]

Fouling increases operational costs as a result of permeate flux decline and/or increased energy consumption because of higher transmembrane pressure (TMP) requirements needed as driving force for the production of drinking water. In

Additional Supporting Information may be found in the online version of this article.

Correspondence concerning this article should be addressed to H. Budman at hbudman@uwaterloo.ca.

addition, frequent chemical cleaning of fouled membranes leads to rapid deterioration of membrane performance, shortened service life, and increased costs. The efficient use of fouling controlling strategies can reduce the energy demand and other operational costs associated with fouling and improve the sustainability of membrane-based drinking water treatment operations to ensure high production of water. This can be accomplished by optimizing the operation of membrane filtration processes.[8]

Methods available for membrane fouling modeling

Optimization of a membrane filtration operation with respect to different variables such as backwashing schedule requires a model that is capable of predicting the extent of reversible and irreversible membrane fouling for given raw water feed. Many studies have focused on achieving this objective by assessing and/or predicting membrane fouling behavior using mechanistic modeling approaches.[9–13] These studies, however, focused mainly on dead-end and a few cross-flow membrane filtration systems that did not involve membrane backwashing cycles, which are typically applied in drinking water treatment systems. Also, these modeling approaches are not suitable for successfully predicting membrane fouling in drinking water applications.

Modeling methods referred to as empirical or black-box approaches such as artificial neural networks,[14,15] empirical models,[16] and genetic programming[17] have also been used to correlate membrane fouling with long-term membrane feed water quality parameters and operation data such as turbidity, temperature, dissolved organic carbon content (DOC), and TMP in pilot-scale filtration studies. As these variables are not always clearly correlated to the evolution of fouling over time, neither these models are able to capture the changes in the different membrane foulant fractions in water during the filtration nor they can relate different fouling behaviors to individual membrane foulant fractions. As a result, the successful implementation of optimization strategies for fouling control based on these black-box models is not always warranted. In addition, from a membrane research standpoint that is geared toward improving membrane fouling characteristics, the aforementioned black-box techniques are not suitable for relating the degree of fouling to the relative concentrations of NOM and other foulant components present in water and, therefore, they are not helpful in addressing remedies for controlling fouling.

Proposed fouling modeling and optimization approach

This study proposes a fluorescence-based modeling approach that is capable of capturing the dynamic changes of different membrane foulant fractions that occur during the UF of natural water for the production of drinking water. This model is developed based on fluorescence excitation–emission matrix (EEM) measurements obtained during UF operation to characterize different membrane foulant components present in water.

Previous studies by the authors have shown that the fluorescence EEM method captures specific fluorescence features that correspond to HS- and protein-like materials[18,19] as well as particulate/colloidal matter[20,21] present in water. The fluorescence EEMs capture a large number of intensity readings recorded at different combinations of excitation and emission wavelengths for natural water samples. Compared to other available NOM membrane foulant characterization methods,[22–24] this approach is capable of differentiating the major membrane foulant fractions and is suitable for performing rapid, direct, and accurate analysis with high instrumental sensitivity.[25,26]

In our previous studies, principal component analysis (PCA) was successfully used to deconvolute spectral information captured within fluorescence EEMs into principal components (PCs) that were related to HS-, protein-like, and colloidal/particulate matter present in natural water.[20,21] As such this PC score-based approach was used as a fault-detection tool for rapid monitoring of the performance of a membrane-based drinking water treatment system. A PCA-based approach was, therefore, used in this study to generate PC scores that correspond to the fluorescence EEMs captured over the course of the UF filtration operation that contained cycles of permeation and membrane backwashing. The novelty of this work as compared to the previous study is that the latent variables corresponding to these PC scores were then used as states within a system of differential equations representing approximate mass balances of the main foulant groups, that is, HS-, protein-like, and colloidal/particulate matter that may be present in water. Thus, the resulting mathematical model can be viewed as a hybrid one where dynamic mass balances are performed over latent variables, whose values are the scores obtained using PCA of experimentally obtained fluorescence EEM data. Based on the UF fouling dynamics predicted by this modeling approach, an optimization strategy is proposed for the estimation of the optimal membrane backwashing scenario that minimizes energy consumption per unit of water produced. The proposed modeling approach is able to forecast/predict membrane fouling behavior ahead of time based on fluorescence measurements obtained earlier during the filtration process and, thus, it is useful for the optimization of membrane filtration operations. This study also demonstrates that this approach can also serve as a membrane research tool by providing an understanding of how major membrane foulant fractions contribute to reversible and irreversible fouling behavior.

Materials and Methods

Grand River water (GRW; Southwestern Ontario, Canada) was filtered using a 200-μm filter (038A-2080; Keller Products, Acton, MA) and used as the feed in UF experiments. The DOC of the feed ranged from 3.9 to 6.5 mg/L and its turbidity values were in the range of 1.2–3.8 nephelometric turbidity units (NTU) during the experimental period (March–November 2009). GRW was stored at 4°C before the experiments and always used within 48 h of the collection time.

Bench-scale membrane filtration set-up

UF experiments were conducted at constant TMP using a bench-scale flat sheet cross-flow set-up as shown in Figure 1. The membrane cross-flow cell holder (Sterlitech CF042; Sterlitech Corporation, Kent, WA) used in this study had an effective membrane area of 42 cm^2. Flat sheet UF

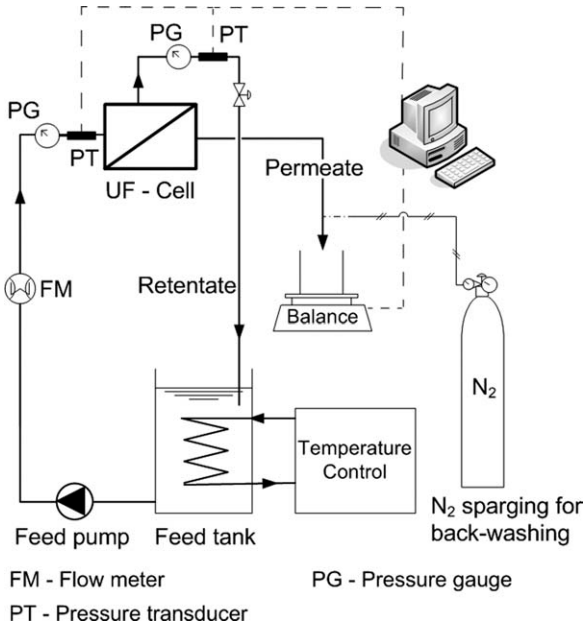

Figure 1. Bench-scale ultrafiltration cross-flow set-up.

membranes with a molecular weight cut-off size of 20 kDa (polysulfone, YMEWSP3001; GE Osmonics) and 60 kDa (polyethersulfone, YMPWSP3001; GE Osmonics) also from Sterlitech Corporation were used. Contact angle measurements performed on virgin 20 and 60 kDa membranes were $72 \pm 2^\circ$ ($n = 6$) and $80 \pm 1^\circ$ ($n = 6$), while the initial pure water fluxes at TMP = 15 psi (103.4 kPa) were ~1.6 and ~2.4 L/(min m^2), respectively. A new membrane was used for each filtration run and prior to the start of each experiment, the membranes were compacted at 15 psi using Milli-Q water until a stable permeate flow was achieved.

Feed water to the membrane set-up was maintained at 0.6 L/min (cross-flow rate) with a TMP of 15 psi. Retentate was circulated back to the feed tank which contained 22 L of water that was maintained at $\sim 25 \pm 1^\circ$C using a temperature controller. This recycle arrangement was used to avoid the need for large amount of water for experimentation. The permeate water was continuously removed and its weight and its corresponding flux values were recorded using a balance connected to a computer using a LabView-based (LabView 8.0; National Instruments, Austin, TX) interface. The filtration consisted of a two-step operation cycle: (1) permeation period and (2) backwashing for 20 s. For comparison purposes, an operation with nonoptimized conditions was used where the permeation period was 1 h while for the optimized backwashing operation the permeation period was determined according to the solution of an optimization problem as will be discussed later. The total filtration time was 267 min for all experiments. During the experimental period, the final flux recorded ranged between 0.66 and 0.78 L/(min m^2) for 20 kDa membranes and 0.70 and 1.22 L/(min m^2) for 60 kDa membranes. Backwashing of the membrane was implemented by forcing the permeate (which is the liquid in the permeate pipe and permeate channels of the membrane cell holder) through the membrane toward the retentate side using nitrogen gas at 10 psi (68.9 kPa). During the backwashing, feed flow was maintained over the membrane surface to induce shear force on the membrane surface, thus, assisting in the removal of foulants. For the purpose of model calibration, fluorescence EEMs of both retentate and permeate were recorded at 15-min intervals during the course of the filtration.

Fluorescence analysis

The fluorescence analysis procedure explained in Peiris et al.[20] was used in this study to record fluorescence EEMs using a Varian Cary Eclipse Fluorescence Spectrofluorometer (Palo Alto, CA). A detailed description of the fluorescence EEM analysis procedure, methods used in fluorescence signal correction, and the selection of the spectrofluorometer parameter settings used in this study for obtaining reproducible fluorescence signals are found in Peiris et al.[20,26,27] During the course of the fluorescence analyses, there were no significant differences in Raman scattering peak intensities recorded for Milli-Q water at Ex/Em ~ 348 nm/396 nm (i.e., difference was less than 2%), confirming that there were no significant fluctuations in the performance of the spectrofluorometer lamp or other hardware. The temperature of the water samples were maintained at room temperature (~25°C) during the analysis. The pH of all the water samples did not change significantly (pH 7.8–8.4) during the experiments and no pH adjustment was made prior to the fluorescence analysis as the fluorescence EEMs are not significantly affected due to small pH differences.[28]

Other analytical methods

The methods used for obtaining DOC, turbidity, and membrane contact angle measurements are as previously described.[21,26]

Fluorescence data pretreatment and principal component analysis

The fluorescence EEM of each sample contained intensity readings at 4214 combinations of excitation and emission wavelengths. The fluorescence intensity values corresponding to all 4214 spectral variables of each EEM were rearranged following the fluorescence EEM data rearrangement procedure described by Peiris et al.[20] This resulted in a $n \times 4214$ fluorescence data matrix, with each row containing fluorescence EEM data of the retentate and permeate for each water sample; n represents the total number of samples composed of both retentate and permeate samples obtained during the UF experiments as described above. This procedure was followed to generate two data matrices referred to as matrix X60 and matrix X20 for UF experiments performed with 60 and 20 kDa membranes, respectively. Then, the X60 and X20 data matrices contained 525 and 560 fluorescence EEMs from 15 and 16 different UF experiments, respectively. PCA was performed on matrix X60 and X20 separately to generate PC scores as explained by Persson and Wedborg,[29] and Peiris et al.[20]

PCA is generally used to extract a smaller set of underlying new variables that are uncorrelated, mutually independent (orthogonal), and that can be mathematically represented by linear combinations of the original variables in the X matrix (X60 or X20 matrix in this case). These new

variables, referred to as PCs or latent variables are able to describe major trends in the original spectral datasets[21] of X60 and X20. PCA decomposes the data matrix X as the sum of the outer product of vectors $\mathbf{s_i}$ and $\mathbf{p_i}$ plus a residual matrix E as presented in Eq. 1.

$$X = \sum_{i=1}^{n} s_i \cdot p_i + \mathrm{E} \tag{1}$$

The $\mathbf{s_i}$ vectors are known as scores (i.e., latent variables' values) on the PCs (i.e., new variables) extracted by PCA. The $\mathbf{p_i}$ vectors are known as loadings and contain information on how the variables (fluorescence variables in this case) relate to each other. By examining the loading values related to each PC, it is possible to understand which original spectral variables in the X matrix are better explained by each PC. A detailed description about PCA can be found elsewhere.[30,31] Before performing PCA analysis, both X60 and X20 matrices were autoscaled by adjusting the columns to zero mean and to unit variance by dividing each column by its standard deviation. To determine the number of PCs that were statistically significant in capturing the underlying features in the X60 and X20 datasets, the leave-one-out cross-validation method[31] was implemented. All computations were performed using the PLS Toolbox 5.2 (Eigenvector Research, Manson, WA) within the MATLAB 7.8.0 computational environment (MathWorks, Natick, MA).

Theoretical basis

The statistically significant PCs calculated as explained above were found to be correlated to different membrane foulants such as HS-like, protein-like, and particulate/colloidal matter present in water (explained later). Thus, the evolution of these PC scores ($\mathbf{s_i}$) corresponding to the PCs is representative of the concentration of the foulant fractions present in water and it can be related to the membrane fouling behavior as demonstrated by Peiris et al.[20,21] The PC scores ($\mathbf{s_i}$) associated with the retentate and permeate of UF processes were, therefore, used to formulate a model of the fouling behavior experienced by 60 and 20 kDa membranes as explained in the following section.

Principal component-based modeling of membrane fouling

As it is currently impossible to quantify each of the individual species in natural water that contribute to fouling it was proposed instead to perform a dynamic balance on the PC scores which were found, as stated above, to be representative of the concentrations of different groups of foulants, that is, HS-like, protein-like, and colloidal/particulate. Thus, the accumulation of membrane foulants on the surface and in the pores of the membrane was calculated based on the PC score balance for a given group of foulants. These mass balances, performed on the control volume of the solution occupied by the membrane, were formulated as a way to account for the mass balances of the individual foulant species present in the water. Accordingly, the accumulation of the membrane foulant (j) that contributes to fouling can, therefore, be represented as follows

$$\frac{ds_{j,\mathrm{M}}}{dt} = \frac{1}{kV_{\mathrm{M}}}\left[(1-w)A\frac{\Delta P}{\mu R_t}(s_{j,\mathrm{R}} - s_{j,\mathrm{P}}) - wL_j\right] \tag{2a}$$

$$L_j = \dot{m}_{\mathrm{wash}}\,\mathrm{eff}_j e^{-q_j R_t} s_{j,\mathrm{M}} \text{ for } j = 1, 2, 4, \ldots, N \text{ and } w = 0 \text{ or } 1 \tag{2b}$$

where s_j is the PC score related to the jth membrane foulant at time $= t$. N is the number of PCs generated by PCA which are statistically significant and deemed to be important for capturing the information related to the major groups of foulants. Subscripts R, P, and M denote retentate, permeate, and the membrane, respectively. V_{M} is the volume of the solution occupied by the membrane and k is a parameter that specifies the active portion of V_{M} (i.e., actual portion of V_{M} that participates in the filtration). The effective membrane surface area, TMP, and the water viscosity are represented by symbols A, ΔP, and μ, respectively. $\dot{m}_{\mathrm{wash}}$ is the volume flow rate used for periodic membrane backwashing, w is a binary variable that models permeation through the membrane ($w = 0$) or backwashing ($w = 1$). eff_j represents the efficiency at which the jth foulant fraction (i.e., foulant fraction related to jth PC) was removed during the backwashing. q_j is a parameter describing the decay of efficiency in backwashing over time due to irreversible fouling caused by the jth membrane foulant. Irreversible fouling is attributed to the accumulated membrane foulant material that cannot be removed by membrane backwashing. R_t is the membrane resistance at time $= t$, which is given in terms of the scores as follows

$$R_t = R_0 + \sum_{j=1}^{N} \beta_j s_{j,\mathrm{M}} + \beta_{\mathrm{inter}} s_{\mathrm{protein,M}} \times s_{\mathrm{coll./partic.,M}} \tag{3}$$

R_0 is the initial membrane resistance before fouling occurs. β_j, $j = 1, 2, 3, \ldots, N$ are the model parameters. β_{inter} is also a model parameter related to the interaction between protein and colloidal/particulate matter (represented by $S_{\mathrm{protein,M}}$ and $S_{\mathrm{coll./partic.,M}}$, respectively) that contributes to membrane fouling. The existence of this interaction was found to be significant in a separate correlation analysis study (results not shown) and found to be very important for improving the model predictions in this study. The significance of incorporating this interaction in the model will be discussed later. It should be noted that while the values of the scores (i.e., s_j values) change with time as per the differential Eq. 2a, the βs are regressed off-line and do not change with time.

Also, the processes involved in the transfer of membrane foulants from the retentate to the membrane or vice versa are quite complex involving deposition of foulants due to attractive forces and removal due to shear stresses acting on the foulant layers. Detailed modeling of these phenomena is difficult. Therefore, it was assumed that the net amount of foulant transfer from the retentate to the membrane is equal to the accumulation of foulants on the surface and in the pores of the membrane as follows

$$D_j(s_{j,\mathrm{R}} - s_{j,\mathrm{M}}) = \frac{\Delta P}{\mu R_t}(s_{j,\mathrm{R}} - s_{j,\mathrm{P}}) \tag{4}$$

where D_j is the effective diffusivity coefficient of the jth foulant fraction. D_{j} is a lumped parameter that combines all possible mass transfer mechanisms involving the transfer of

membrane foulants from the retentate to the membrane or vice versa as mentioned above.

The permeate water flux through the membrane at time = t is as follows

$$J_t = \frac{\Delta P}{\mu R_t} \tag{5}$$

The general rationale behind Eqs. 2a and 2b is that if the fluorescence intensities would be related linearly to the compositions of the individual foulant species, these equations would constitute actual dynamic balances for each species. Moreover, if the fouling resistance would be constant for all species and the PCs would capture the majority of foulants present in the water, the combination of Eqs. 2a and 2b will result in an overall mass balance of foulants for the membrane. However, as the combination of Eqs. 2a, 2b, and 3 is nonlinear with respect to the scores, the model above is only an approximation to an actual mass balance of foulants. Thus, ultimately the model has to be calibrated by input–output data as explained in the following section to result in accurate predictions of fouling resistance with respect to the PCs information based on fluorescence.

Model calibration and validation

Experimental permeate water flux data obtained by UF runs performed using GRW with different DOC content and turbidity values within the ranges as indicated above were used to calibrate the state space model given by the system of Eqs. 2a, 2b, 3, and 5. The model calibration involved the estimation of the model parameters k, β_1, β_2, β_3, …, β_N, $\beta_{\text{inter.}}$, eff_1, eff_2, eff_3, …, eff_N and q. This was achieved by minimizing the sum of squares error (SSE) between experimental and model estimations of permeate water flux by using the MATLAB function "ga," a genetic algorithm code available within the MATLAB 7.8.0 computational environment. Model parameters, estimated in separate model calibrations for 60 and 20 kDa UF membranes, are listed in the Supporting information Table S-1. It should be noted that this calibration involved 140 permeate flux measurement data points recorded over the duration of filtration per each filtration run considered. Five filtration runs, each for 60 and 20 kDa UF membranes corresponding to different fouling behaviors were used for calibration. The model calibration results can be found in Supporting information. The model estimations were generated using the PC scores of retentate ($s_{j,\text{R}}$) and permeate ($s_{j,\text{P}}$) that correspond to fluorescence EEM measurements, obtained every 15 min during the course of UF. These scores were used as inputs to Eqs. 2a and 2b whereas the output was the corresponding score value of the accumulated foulant fraction j at the membrane, $s_{j,\text{M}}$calculated from Eq. 2a. The MATLAB ordinary differential equation (ODE) solver "ode23" was used in solving the above state space model. Model validation was achieved using additional experimental permeate water flux and fluorescence EEMs data that were not used in the calibration. UF experimental data with low, medium, and high fouling events involving data from a total of nine and 10 experiments for 60 and 20 kDa UF membranes, respectively, were used for model validation. The high and low fouling situations correspond to the highest and lowest flux decline recorded (at the end of the filtration) during the experimental period. The medium-level fouling events correspond to experiments where the flux decline was at an intermediate level between the highest and lowest fouling events. It should be noted that feed water with high DOC content and turbidity generally resulted in high fouling situations for both membranes. These feed water quality parameters are reported in our previous work.[21]

Generation of model predictions

The model given by the system of Eqs. 2a, 2b, 3, 4, and 5 was then used to obtain model predictions based solely on the fluorescence EEMs of retentate and permeate captured at time = 15 min after the start of the UF experiments. PC scores ($s_{j,\text{R\_15 min}}$ and $s_{j,\text{p\_15 min}}$) that are related to these fluorescence measurements were used for the estimation of the predicted permeate water flux into the future along a total time horizon of 4 h. During the calculations of model predictions, the PC scores related to the retentate were assumed to be constant and equal to the values obtained at time = 15 min during the prediction period (i.e., $s_{j,\text{R}} = s_{j,\text{R\_15 min}}$ in Eq. 4). This assumption was based on the very small changes (<5% increase in most cases) in the PC scores of retentate observed during the UF experiments. Also, the initial estimations of the effective diffusivity coefficient D_j (j = 1, 2, 3, …, N) was calculated using Eq. 4 based on PC scores corresponding to the fluorescence EEMs of retentate and permeate captured at time = 15 min. These initial estimations were subsequently updated according to the following empirical recursive function (Eq. 6) during the calculation of model predictions to account for the change of D_j resulting from membrane fouling over time. The recursive updating of the D_j were not based on any other subsequent fluorescence EEM measurements obtained at time >15 min.

This was deemed to be necessary for approximating the evolving fouling conditions over time; without this approach for updating D_j, model predictions deviated significantly (prediction error >20%) from the experimental values.

$$D_{j,t} = z_1 D_{j,}\text{int} + z_2 D_{j,t-\Delta t} \quad \text{for} \quad J = 1, 2, 3, \ldots, N \tag{6}$$

where $D_{j,t}$ is the effective diffusivity coefficient of the jth foulant fraction at time $t = t$, $D_{j,\text{int}}$ = is the initial estimate of D_j and $D_{j\ t\ -\Delta t}$ is the value of D_j at time $t = t - \Delta t$. Δt is the constant time step length (Δt = 1 s) used by the ODE solver. Z_1 and Z_2 are parameters that were estimated by minimizing the SSE between model predictions and measured permeate water flux using a genetic algorithm approach as mentioned above. It should also be noted that Eq. 6 does not necessarily cause D_j to increase over time. As the accumulation of foulant content in the membrane increases, the removal of foulants from the membrane to the retentate becomes significant, causing D_j to decrease as per Eq. 4. The prediction ability of the model was also validated with additional experimental permeate water flux and fluorescence EEM data that were not used in estimating the Z_1 and Z_2 parameters (model validation data will be presented and discussed later).

Table 1. Variance Captured in the PCA of the X60 and X20 Matrices

Principal Component	X60 Matrix (60 kDa UF Spectral Data)		X20 Matrix (20 kDa UF Spectral Data)	
	Variance Captured (%)	Related Membrane Foulant	Variance Captured (%)	Related Membrane Foulant
1	63.0	Humic substances	75.0	Humic substances
2	16.4	Colloidal/particulate	9.6	Colloidal/particulate
3	5.5	Protein-like	6.1	Protein like
4	4.7	Colloidal/particulate	–	–
Total	89.6		90.7	

Optimization of the ultrafiltration process

The predicted permeate water flux can be used to understand the extent of fouling of the membrane and the reduced permeate water flux occurring over time for constant TMP operations (as demonstrated in this study). On the other hand, if constant permeate flux is desired, the TMP should be gradually increased to compensate for the increasing resistance as a result of fouling. In both situations, membrane fouling results in an increase in the energy requirement per unit amount of drinking water produced.

In this study, the UF membrane backwashing times were used as optimization variables to optimize the UF process so that the energy requirement per unit amount of drinking water produced was minimized. This optimization approach was implemented by minimizing the following objective function (OF) with respect to backwashing times (Eq. 7) subjected to the constraints listed in Eqs. 10 and 11.

$$\min_{t_1,t_2,t_3,t_4}\left(\mathrm{OF}=\frac{\text{energy consumption}}{\text{water production}}\right) \tag{7}$$

where energy consumption and the water production for time duration $=\Delta t$ is given by

$$\text{Energy consumption}=\frac{A(\Delta P)^2\Delta t}{\mu R_t} \tag{8}$$

$$\text{Water production}=J_t A\Delta t \tag{9}$$

$$\begin{bmatrix}1 & -1 & 0 & 0\\ 0 & 1 & -1 & 0\\ 0 & 0 & 1 & -1\\ 0 & 0 & 0 & 1\end{bmatrix}\begin{bmatrix}t_1\\ t_2\\ t_3\\ t_4\end{bmatrix}\le\begin{bmatrix}-t_w\\ -t_w\\ -t_w\\ t_F-t_w\end{bmatrix} \tag{10}$$

$$t_1\ge t_d \tag{11}$$

where t_1, t_2, t_3, and t_4 are the times at which the backwashing of the UF membrane was implemented. The number of backwashing cycles was limited to four for the purpose of demonstrating the application of the proposed approach. On the other hand, the number of backwashes represent another parameter that could be included in this optimization approach but this will be addressed in future research. Also, $t_w = 180$ s is the sum of the time needed for backwashing (20 s) and the time required to connect and disconnect the nitrogen gas supply for backwashing and for adjusting the TMP of the UF membrane cell holder (160 s), which were performed manually. The total filtration time is indicated by t_F (= 267 min), and t_d (= 15 min) is the time at which the first set of fluorescence EEMs of the retentate and permeate for UF operation were collected. This information was required for the model predictions as explained before. The minimization of the OF (Eq. 7) subjected to the constraints (Eqs. 10 and 11) were performed by using the MATLAB function "ga."

Results and Discussion

Typical fluorescence spectral features of Grand River water

The fluorescence EEMs of GRW used in this study exhibited fluorescence regions that are representative of the presence of major membrane foulants such as HS- (at excitation wavelength (Ex) ~320 nm and emission wavelength (Em) ~ 415 nm) and protein-like (at Ex/Em ~ 280 nm/330 nm) NOM.[20,21] These results are also consistent with fluorescence EEM data published elsewhere.[18,23,25,32,33] The presence of HS- and protein-like matter in GRW was also previously confirmed by liquid chromatography-organic carbon detection (LC-OCD) analysis.[20,25] In addition, Rayleigh scattering (RS) regions observed in the fluorescence EEMs of GRW can also provide information related to the particulate/colloidal matter.[20] Typical fluorescence EEM spectra of GRW—similar to the ones recorded in this study—that indicate the aforementioned regions have been previously reported[20,26] and are, therefore, not presented here but are included in Supporting information Figure S-2.

Principal component analysis of fluorescence data

PCA of X60 and X20 matrices generated four and three statistically significant PCs, respectively, capturing nearly 90% of the total variance present in the original spectral variables obtained from 60 and 20 kDa UF experiments (Table 1). These PCs were found to be related to different membrane foulant fractions present in water as shown in Table 1. This was verified by examining the loading plots corresponding to each PC (generated from the loading values, i.e., $\mathbf{p_i}$ values) as demonstrated by Peiris et al.[21] The loading plots of each PC corresponding to 60 kDa UF experiments are shown in Figure 2a–d. For example, the loading peak regions α' and β' of PC-1 appeared in the same location where the fluorescence EEM regions related to HS-like NOM. Similar observations were made with the loading peak regions (RS′) for PC-2, peak δ' for PC-3, and loading peak regions (RS′) for PC-4 in relation to the foulant fractions they represent as indicated in Table 1. Comparable loading plots were also seen for each PC corresponding to 20 kDa UF experiments and can be found in Supporting information Figure S-3. The remaining variance (~10%) in each case was considered to be due to the combination of unexplained variance by these PCs and the instrumental

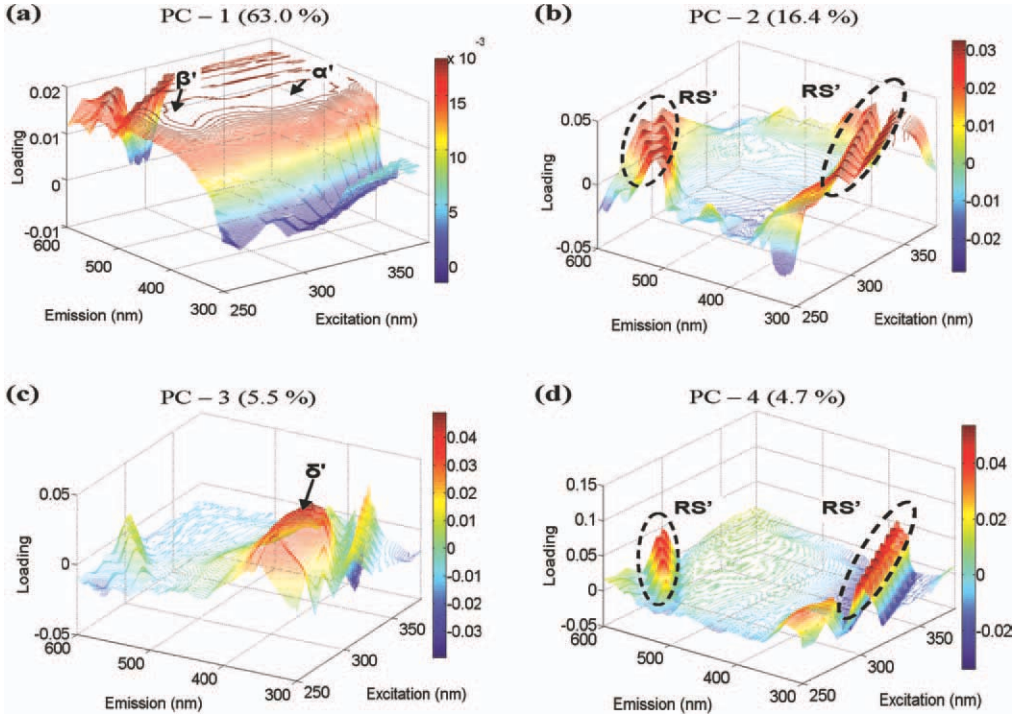

Figure 2. Three-dimensional illustrations of the loading matrices of (a) PC-1, (b) PC-2, (c) PC-3, and (d) PC-4 generated by the PCA of 60 kDa filtration data.

Rayleigh scattering peak-like regions (RS′) are indicated in dashed circles. Variance captured by each PC is indicated within parentheses. [Color figure can be viewed in the online issue, which is available at wileyonlinelibrary.com.]

noise (determined to be less than 5% of the intensity readings) in the fluorescence measurements. Although it is possible to capture the remaining variance by generating additional PCs, additional PCs were not found to be related to any major membrane foulant fractions present in water (see Table 1).

Model predictions and validation

Model predictions and the experimentally measured normalized permeate water flux of selected 60 and 20 kDa UF experiments that were not used in the model calibration/parameter estimation are shown in Figure 3. Permeate flux was normalized with respect to initial pure water flux of the membranes. These experiments correspond to low, medium, and high membrane fouling situations. The sudden increases in permeate flux occurring immediately after the exponential-type flux declines of the permeation steps correspond to the membrane backwashing steps. The model predictions for these experiments were obtained using only the fluorescence-based PC scores of retentate and permeate obtained at time = 15 min from the start of the UF as explained earlier. The permeate flux prediction results indicate that the model was able to successfully predict different membrane fouling behaviors experienced by both UF membrane types. The root mean-squared error between predictions and experimental values for high, medium, and low fouling situations were 0.004, 0.016, and 0.021, respectively, for 60 KDa UF operations and 0.005, 0.013, and 0.010, respectively, for 20 kDa UF operations.

These results indicate that the proposed fouling modeling approach can be used for forecasting different fouling behaviors corresponding to changes in the membrane feed water quality. Hence, this modeling approach can be used to predict the evolution of fouling well in advance and, thus, appropriate model-based optimization measures can be implemented.

Significance of interaction between protein and colloidal/particulate matter in model predictions

Our previous work that involved fluorescence analysis of permeate and retentate samples, obtained during the UF of GRW, indicated possible existence of colloidal/particulate–protein interactions.[21] In addition, Susanto et al.[34] indicated that polysaccharide-like matter contained in the colloidal/particulate fraction of water can interact with protein-like matter and contribute synergistically toward membrane fouling. Because of these reasons, the impact on model predictions by the interaction between colloidal/particulate and protein-like matter was examined. This interaction was represented in the model in the form of "$S_{\text{protein,M}} \times S_{\text{coll./partic.,M}}$" as described earlier. As a result of including this interaction term in the model, model predictions improved for all fouling situations, with most considerable improvements observed for high fouling situations. Figure 4a and b demonstrates the model predictions for high fouling situations obtained with and without incorporating $S_{\text{protein,M}} \times S_{\text{coll./partic.,M}}$ in the model for 60 and 20 kDa experiments. When the interaction between colloidal/particulate and protein-like matter was considered, better model prediction for the normalized permeate water flux was

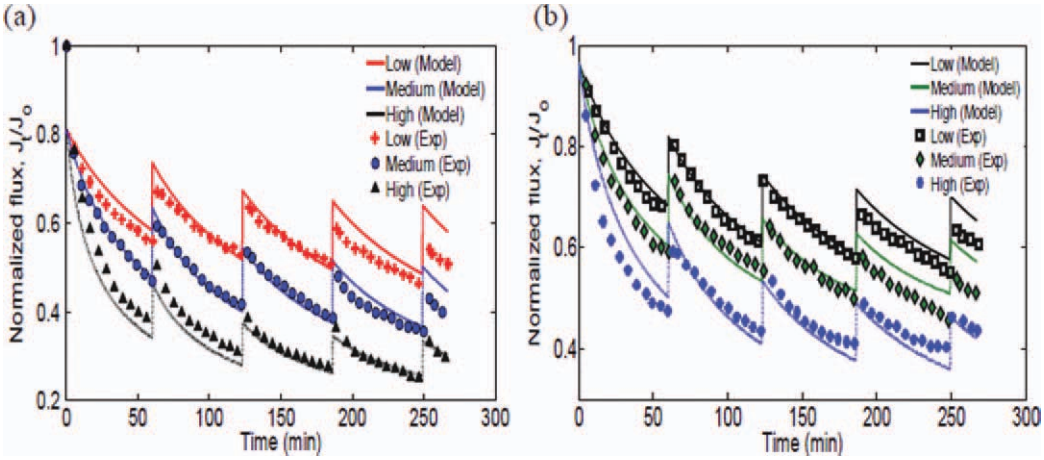

Figure 3. Model predictions (lines) and experimentally measured (symbols) normalized permeate water flux for selected (a) 60 kDa and (b) 20 kDa UF experiments of low, medium and, high membrane fouling situations.

[Color figure can be viewed in the online issue, which is available at wileyonlinelibrary.com.]

obtained. The improvements in the root mean-squared error between predictions and experimental values were from 0.08 to 0.004 and 0.012 to 0.005 for 60 and 20 kDa filtration experiments, respectively, indicating the importance of incorporating the interaction between colloidal/particulate and protein-like matter in the model.

Optimization of ultrafiltration for drinking water treatment

The proposed modeling approach was then applied for the optimization of 60 and 20 kDa UF operations as explained before. GRW obtained on October 25 and November 23, 2009 was used in the 60 and 20 kDa experiments, respectively.

Figure 3a and b demonstrates the model predictions of the fouling behavior for UF of GRW (prefiltered) using 60 and 20 kDa membranes with backwashing at regular time intervals of 1 h (i.e., before implementing optimal backwashing intervals). When backwashing times were optimized using the proposed optimization approach for the 60 kDa membrane, the model predictions indicated energy savings of 3.7% with a 4.3% increase in the total volume of drinking water production. The backwashing times generated by the optimization approach were $t_1 = 61$ min, $t_2 = 90$ min, $t_3 = 118$ min, and $t_4 = 137$ min. Applying the same approach for the 20 kDa membrane, it was shown that it is possible to achieve energy savings of 2.6% with a 3.1% increase in the total volume of water production. The corresponding optimum backwashing times for the 20 kDa membrane were $t_1 = 69$ min, $t_2 = 97$ min, $t_3 = 132$ min, and $t_4 = 172$ min. The optimal backwashing cycles were implemented experimentally to test the validity of the optimization results. The results of these experiments are shown in Figure 5a and b indicating very good agreement between experimental values and model predictions, thus, confirming the optimization solution.

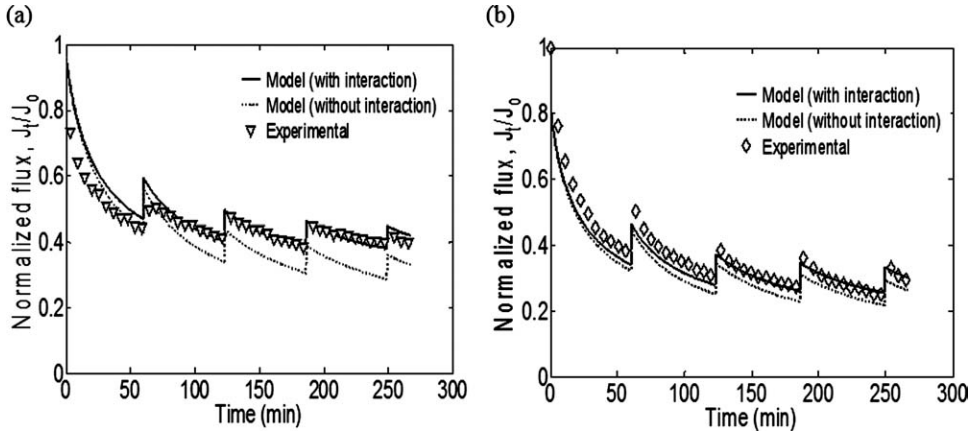

Figure 4. Model predictions (lines) and experimentally measured (symbols) normalized permeate water flux for (a) 60 kDa and (b) 20 kDa UF experiments of high membrane fouling situations.

Predictions obtained with (solid lines) and without (broken lines) incorporating the interaction between colloidal/particulate and protein-like matter are denoted.

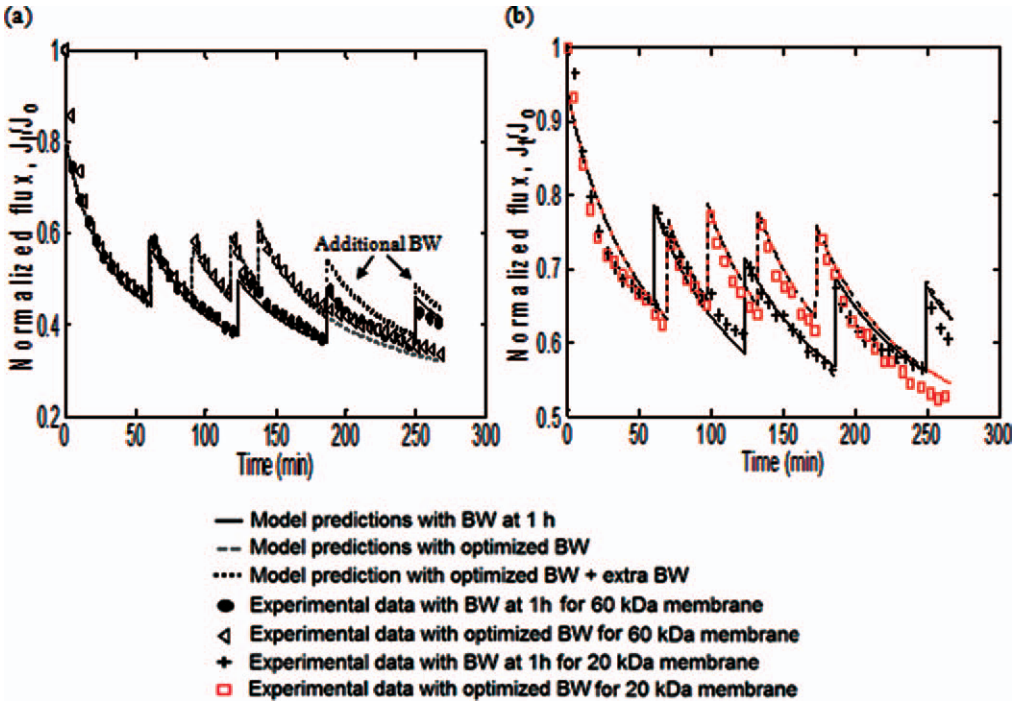

Figure 5. Model predictions (lines) and experimentally measured (symbols) normalized permeate water flux obtained for (a) 60 kDa and (b) 20 kDa UF operations with normal backwashing (BW) times (every hour) and optimized backwashing times.

[Color figure can be viewed in the online issue, which is available at wileyonlinelibrary.com.]

Although the optimization approach developed in this study was limited to four backwashing cycles, it is possible to further improve the energy savings and the water production by using additional backwashing cycles with the optimized conditions. For example, when two additional backwashing cycles, for which backwashing times were selected arbitrarily, were included as illustrated in Figure 5a, the model predictions indicated an increase in the energy savings and the volume of drinking water production up to ~8.0% and ~9.8%, respectively. In general, it is expected that the use of additional backwashing cycles will also limit the high fouling behavior of the membrane that may occur even when the optimized backwashing, as observed in this study, was implemented toward the end of the filtration. In addition, it is expected that optimal operation would further extend the life span of the membrane and minimize the need for chemical cleaning to recover flux decline caused by irreversible fouling.

In this study, the optimization of the filtration process was limited to ~4 h due to the practical and time constrains in running the filtration experiment in a lab environment with fresh natural water. The UF experiments were run at room temperature and, thus, preservation of feed water for a longer period was not possible. Each filtration experiment required additional 6 h for sample preparation (warming up the water to room temperature after overnight storage in a cold room and prefiltration), compaction of the new membrane prior to the experiment, and fluorescence analysis of the feed/retentate and permeate water samples. For these reasons, filtration experiments with longer time periods were not practically possible. This limited the time available for optimization of the filtration operation to up to ~4 h. However, in industrial filtration systems, these constraints could be eliminated with the availability of using natural water as the feed water directly from the source and by possibly implementing in-line fluorescence measurements. In such situations, longer optimization periods become realistic and additional backwashing cycles could be incorporated in this proposed approach to maximize the energy saving and the volume of drinking water production. To this end, current research is investigating the number of backwashing cycles as another optimization parameter, during a moving time window, for the optimization of longer and continuous filtration operations.

The ability of this modeling approach to reasonably predict the reversible and irreversible fouling behavior experienced by both membranes with backwashing time intervals that are different to those used in the model calibration indicate that the proposed approach is generally robust in modeling different—generally unplanned or infrequent—filtration situations which are difficult to model. However, model predictions generally appeared to slightly deviate from the experimental flux measurements toward the end of the filtration experiments. This was somewhat expected as the model predictions are based on a single time interval of fluorescence EEMs measurement obtained at time = 15 min from the start of the UF experiments. This inaccuracy will be addressed in future studies by using additional fluorescence EEM measurements, obtained during past and current filtration periods (i.e., sampling time for fluorescence analysis <

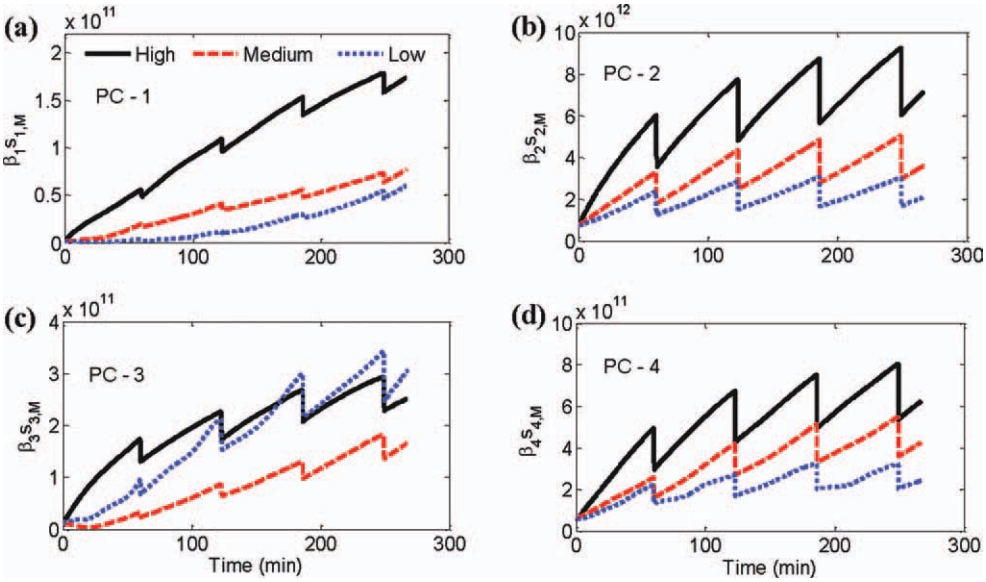

Figure 6. The contribution of (a) humic substances (HS)-like (PC-1), (b and d) colloidal/particulate (PC-2 and PC-4) and (c) protein-like (PC-3) matter on membrane resistance as calculated in terms of the accumulation of individual foulant components in/on the membranes for selected 60 kDa UF experiments of low, medium, and high membrane fouling situations.

[Color figure can be viewed in the online issue, which is available at wileyonlinelibrary.com.]

time at which the model prediction are generated). This frequently updated model would produce better predictions over future time horizons.

Role of membrane foulant components in reversible and irreversible fouling

Another important aspect of the modeling approach developed in this study is that it can be used to estimate the accumulation of individual foulant components in/on the membranes in terms of the PC scores (i.e., $s_{j,\mathrm{M}}$; where j is the PC related to the jth foulant component) as illustrated in Eqs. 2a and 2b. These individual membrane foulant components contribute differently to the increase in the membrane resistance (R_t) and this relative contribution can be quantified by the value of $\beta_j s_{j,\mathrm{M}}$ for each foulant component (j) in Eq. 3. Therefore, by examining the evolution of $\beta_j s_{j,\mathrm{M}}$ (for $j = 1, 2, 3, 4$), one can assess how different membrane fouling components, identified in this study, contribute to membrane fouling. Figure 6a–d illustrates the evolution of these estimates for the main foulant components, such as HS-like, protein-like, and colloidal/particulate matter for high, medium, and low fouling events experienced by 60 kDa membranes. Similar observations were made for 20 kDa membranes (results not shown for brevity). The corresponding PCs are also indicated in Figure 6.

It should be noted that these estimates were calculated using the PC scores related to fluorescence EEMs of retentate and permeate obtained during the course of the UF experiments using Eqs. 2a, 2b, and 3. Thus, these model estimates obtained through Eq. 2a with actual fluorescence data collected along the experiment are representative of the foulant accumulation on the membranes during the course of the 60 kDa UF experiments.

The cyclical drops in $\beta_j s_{j,\mathrm{M}}$ values in Figure 6a–d are correlated with the flux increase or alternatively fouling decrease obtained after each membrane backwashing as illustrated in Figure 3. Based on the relatively larger changes observed after backwashing for PC-2 and PC-4, one can conclude that colloidal/particulate matter accumulated in/on the membranes was removed predominantly by backwashing compared to HS- and protein-like foulants. As a result, colloidal/particulate matter demonstrates a comparatively larger contribution to reversible fouling. HS- and protein-like foulants on the other hand are seen to be contributing significantly toward irreversible fouling (i.e., smaller drop in $\beta_1 s_{1,\mathrm{M}}$ and $\beta_2 s_{2,\mathrm{M}}$ values after backwashes). These observations are consistent with previous interpretations provided for reversible and irreversible UF fouling by river water foulant extracts[35,36] and model foulants.[37,38] In addition, in a separate study that involved the same filtration procedure, membranes and feed water samples, foulant components that was deposited in the pores and/or on the surface of the membranes were extracted and characterized using fluorescence spectroscopy.[21] This study also confirmed the above model-based observations related to the fouling behavior of HS-, protein-like, and colloidal/particulate matter. Therefore, it can be concluded that the proposed modeling approach allows identification of the type of foulant components in the water that are contributing to reversible and irreversible fouling eliminating the need to perform membrane autopsy analyses which are often difficult and time consuming. In addition to drinking water treatment-related membrane applications, this approach could also have application in other types of membrane-based treatment or separation of substances that have fluorescence properties.

Conclusions

The proposed fluorescence-based membrane fouling modeling approach was found suitable for accurately predicting different fouling situations for UF cross-flow treatment of river water. Model forecasts/predictions along a prediction horizon of several hours are based on the fluorescence EEM measurements captured at time = 15 min of the UF operation and this provides sufficient time for fouling optimization strategies in terms of scheduling of backwashing and chemical cleaning (to recover membrane permeability due to irreversible fouling) to be implemented. The approach is especially important for forecasting high fouling events that are often harmful for membranes or challenging for the efficient production of drinking water to meet consumer demand. The ability of this approach for process optimization in terms of minimizing the energy spent per unit amount of drinking water produced was demonstrated. In addition, the proposed approach is also able to identify specific membrane foulants that contribute to reversible and irreversible fouling of membranes in drinking water applications and as such, it is a useful tool for membrane research. The proposed approach is significant in the context that most available approaches for modeling and prediction of membrane fouling use typical feed water quality parameters and operation data such as turbidity, temperature, DOC, and TMP as monitoring variables, which poorly correlate with the evolution of fouling over time and as a result are inadequate for predicting fouling situations that result from abrupt changes in the feed water quality.

Acknowledgments

Funding for this work from the Canadian Water Network and the Natural Sciences and Engineering Research Council of Canada (NSERC) is gratefully acknowledged.

Literature Cited

1. Fiksdal L, Leiknes T. The effect of coagulation with MF/UF membrane filtration for the removal of virus in drinking water. *J Membr Sci*. 2006;279:364–371.
2. Ordonez R, Hermosilla D, Pio IS, Blanco A. Evaluation of MF and UF as pretreatments prior to RO applied to reclaim municipal wastewater for freshwater substitution in a paper mill: a practical experience. *Chem Eng J*. 2011;166:88–98.
3. Farahbakhsh K, Smith DW. Membrane filtration for cold regions—impact of cold water on membrane integrity monitoring tests. *J Environ Eng Sci*. 2006;5:S69–S75.
4. Saravia F, Zwiener C, Frimmel FH. Interactions between membrane surface, dissolved organic substances and ions in submerged membrane filtration. *Desalination*. 2006;192:280–287.
5. Jermann D, Pronk W, Meylan S, Boller M. Interplay of different NOM fouling mechanisms during ultrafiltration for drinking water production. *Water Res*. 2007;41:1713–1722.
6. Ebrahim S. Cleaning and regeneration of membranes in desalination and wastewater applications: state-of-the-art. *Desalination*. 1994;96:225–238.
7. Kimura K, Hane Y, Watanabe Y. Effect of pre-coagulation on mitigating irreversible fouling during ultrafiltration of a surface water. *Water Sci Technol*. 2005;51:93–100.
8. Seidel A, Elimelech M. Coupling between chemical and physical interactions in natural organic matter (NOM) fouling of nanofiltration membranes: implications for fouling control. *J Membr Sci*. 2002;203:245–255.
9. Bowen WR, Calvo JI, Hernandez A. Steps of membrane blocking in flux decline during protein microfiltration. *J Membr Sci*. 1995;101:153–165.
10. Tansel B, Bao WY, Tansel IN. Characterization of fouling kinetics in ultrafiltration systems by resistances in series model. *Desalination*. 2000;129:7–14.
11. Chang Y, Benjamin MM. Modeling formation of natural organic matter fouling layers on ultrafiltration membranes. *J Environ Eng*. 2003;129:25–32.
12. Taniguchi M, Kilduff JE, Belfort G. Modes of natural organic matter fouling during ultrafiltration. *Environ Sci Technol*. 2003;37:1676–1683.
13. Bolton G, LaCasse D, Kuriyel R. Combined models of membrane fouling: development and application to microfiltration and ultrafiltration of biological fluids. *J Membr Sci*. 2006;277:75–84.
14. Delgrange-Vincent N, Cabassud C, Cabassud M, Durand-Bourlier L, Laine JM. Neural networks for long term prediction of fouling and backwash efficiency in ultrafiltration for drinking water production. *Desalination*. 2000;131:353–362.
15. Cabassud M, Delgrange-Vincent N, Cabassud C, Durand-Bourlier L, Laine JM. Neural networks: a tool to improve UF plant productivity. *Desalination*. 2002;145:223–231.
16. Shengji X, Juanjuan Y, Naiyun G. An empirical model for membrane flux prediction in ultrafiltration of surface water. *Desalination*. 2008;221:370–375.
17. Lee T, Oh H, Choung Y, Oh S, Jeon M, Kim J, Nam SH, Lee S. Prediction of membrane fouling in the pilot-scale microfiltration system using genetic programming. *Desalination*. 2009;247:285–294.
18. Baker A. Fluorescence excitation–emission matrix characterization of some sewage-impacted rivers. *Environ Sci Technol*. 2001;35:948–953.
19. Henderson RK, Baker A, Murphy KR, Hambly A, Stuetz RM, Khan SJ. Fluorescence as a potential monitoring tool for recycled water systems: a review. *Water Res*. 2009;43:863–881.
20. Peiris RH, Halle C, Budman H, Moresoli C, Peldszus S, Huck PM, Legge RL. Identifying fouling events in a membrane-based drinking water treatment process using principal component analysis of fluorescence excitation–emission matrices. *Water Res*. 2010;44:185–194.
21. Peiris RH, Budman H, Moresoli C, Legge RL. Understanding fouling behaviour of ultrafiltration membrane processes and natural water using principal component analysis of fluorescence excitation–emission matrices. *J Membr Sci*. 2010;357:62–72.
22. Huber SA, Frimmel FH. A liquid chromatographic system with multidetection for the direct analysis of hydrophilic organic compounds in natural waters. *Fresenius J Anal Chem*. 1992;342:198–200.
23. Her N, Amy G, McKnight D, Sohn J, Yoon Y. Characterization of DOM as a function of MW by fluorescence EEM and HPLC-SEC using UVA, DOC, and fluorescence detection. *Water Res*. 2003;37:4295–4303.
24. Gray SR, Ritchie CB, Tran T, Bolto BA. Effect of NOM characteristics and membrane type on microfiltration performance. *Water Res*. 2007;41:3833–3841.
25. Coble PG, Green SA, Blough NV, Gagosian RB. Characterization of dissolved organic matter in the Black Sea by fluorescence spectroscopy. *Nature*. 1990;348:432–435.
26. Peiris BRH, Halle C, Haberkamp J, Legge RL, Peldszus S, Moresoli C, Budman H, Amy G, Huck PM. Assessing nanofiltration fouling in drinking water treatment using fluorescence fingerprinting and LC-OCD analyses. *Water Sci Technol: Water Supply*. 2008;8:459–465.
27. Peiris BRH, Budman H, Moresoli C, Legge RL. Acquiring reproducible fluorescence spectra of dissolved organic matter at very low concentrations. *Water Sci Technol*. 2009;60:1385–1392.
28. Spencer RGM, Bolton L, Baker A. Freeze/thaw and pH effects on freshwater dissolved organic matter fluorescence and absorbance properties from a number of UK locations. *Water Res*. 2007;*41*:2941–2950.
29. Persson T, Wedborg M. Multivariate evaluation of the fluorescence of aquatic organic matter. *Anal Chim Acta*. 2001;434:179–192.
30. Wold S, Esbensen K, Geladi P. Principal components analysis. *Chemom Intell Lab Syst*. 1987;2:37–52.
31. Eriksson L, Johansson E, Kettaneh-Wold N, Wold S. *Multi- and Megavariate Data Analysis, Principles and Applications*. Umea, Sweden: Umetrics Academy, 2001, ISBN 91-973730-1-X, p. 533.

32. Chen W, Westerhoff P, Leenheer JA, Booksh K. Fluorescence excitation–emission matrix regional integration to quantify spectra for dissolved organic matter. *Environ Sci Technol*. 2003;37:5701–5710.
33. Sierra MMD, Giovanela M, Parlanti E, Soriano-Sierra EJ. Fluorescence fingerprint of fulvic and humic acids from varied origins as viewed by single-scan and excitation/emission matrix techniques. *Chemosphere*. 2005;58:715–733.
34. Susanto H, Arafat H, Janssen EML, Ulbricht M. Ultrafiltration of polysaccharide–protein mixtures: elucidation of fouling mechanisms and fouling control by membrane surface modification. *Sep Purif Technol*. 2008;63:558–565.
35. Jucker C, Clark MM. Adsorption of aquatic humic substances on hydrophobic ultrafiltration membranes. *J Membr Sci*. 1994;97:37–52.
36. Aoustin E, Schäfer AI, Fane AG, Waite TD. Ultrafiltration of natural organic matter. *Sep Purif Technol*. 2001;22–23:63–78.
37. Jones KL, O'Melia CR. Ultrafiltration of protein and humic substances: effect of solution chemistry on fouling and flux decline. *J Membr Sci*. 2001;193:163–173.
38. Jermann D, Pronk W, Kagi R, Halbeisen M, Boller M. Influence of interactions between NOM and particles on UF fouling mechanisms. *Water Res*. 2008;42:3870–3878.

Manuscript received Feb. 16, 2011, and revision received May 6, 2011.